Abstracts

CATALYSIS – APPLIED AND PHYSICAL ASPECTS

Fabrication of Noble-Metal Catalysts with a Desired Surface Wettability and Their Applications in Deciphering Multiphase Reactions

D. Wang, S. Wang, H. Jin, W. Zhang, Y. Yang, A. Sun, T. Tang and J. Wang, *ACS Appl. Mater. Interfaces*, 2013, **5**, (9), 3952–3958

Pt and Pd catalysts with a wide range of surface wettabilities were fabricated through an electrochemical method and were characterised with SEM, EDX spectroscopy, TEM and AFM. No surfactant was required. The control of the macroscopic properties of the Pt and Pd catalyst layers led to very different performances in the electrooxidation of hydrogen peroxide and sodium formate or the reduction of oxygen in alkaline solutions. This study demonstrated that wettability not only influences the performance of a solid catalyst, but can also help decipher multiphase reaction mechanisms.

Ru Particle Size Effect in Ru/CNT-Catalyzed Fischer-Tropsch Synthesis

J. Kang, W. Deng, Q. Zhang and Y. Wang, *J. Energy Chem.*, 2013, **22**, (2), 321–328

CNT-supported Ru NPs with mean sizes 2.3 nm to 9.2 nm were prepared using different post-treatments and investigated for Fischer-Tropsch synthesis. With shorter contact times, the TOF for CO conversion was dependent on the mean size of the Ru particles; TOF increased with the mean size of Ru particles from 2.3 nm to 6.3 nm and then decreased slightly. The selectivities to C_{5+} hydrocarbons increased gradually with the mean size of Ru particles up to 6.3 nm and then remained almost unchanged with a further increase in Ru particle size. With longer contact times, C_{10}–C_{20} selectivity increased significantly at the expense of C_{21+} selectivity.

Confinement of the Grubbs Catalyst in Alkene-Functionalized Mesoporous Silica

H. Staub, F. Kleitz and F.-G. Fontaine, *Microporous Mesoporous Mater.*, 2013, **175**, 170–177

Grubbs I catalyst, $[RuCl_2(=C(H)(Ph))(PCy_3)_2]$, was incorporated into ordered mesoporous SBA-15 silica materials functionalised with alkenyl-trichlorosilanes with different C chain lengths, e.g. vinyl- (C_2), allyl- (C_3), hexenyl- (C_6) and octenyl- (C_8) trichlorosilanes. The obtained materials, before and after interaction with Grubbs I, were characterised and the investigations revealed a pronounced dependence of the Grubbs catalyst stability on the alkyl chain length of the grafted moieties. The nature of the immobilised Ru-based species was a function of the surface modification, i.e. chain length of the alkenyl-silane.

CATALYSIS – INDUSTRIAL PROCESS

Rapid Analysis of Residual Palladium in Pharmaceutical Development Using a Catalysis-Based Fluorometric Method

X. Bu, K. Koide, E. J. Carder and C. J. Welch, *Org. Process Res. Dev.*, 2013, **17**, (1), 108–113

A fast and inexpensive high-throughput approach has been found for the detection of residual Pd in pharmaceutical intermediates to support laboratory or pilot plant Pd removal. The approach was based on the Pd-catalysed Tsuji–Trost deallylation of an allylic ether substrate to produce a highly fluorescent product. Excellent sensitivity and linearity were found with Pd standards, and a reasonably good ability to quantify Pd (80–110% of actual) was observed for samples in which appropriate pretreatments with *aqua regia* and $NaBH_4$ were performed. A streamlined assay procedure involving a predispensed reagent cocktail that was stable for a day at room temperature (and for months in the freezer) is described.

Industrial Scale-Up of Enantioselective Hydrogenation for the Asymmetric Synthesis of Rivastigmine

P.-C. Yan, G.-L. Zhu, J.-H. Xie, X.-D. Zhang, Q.-L. Zhou, Y.-Q. Li, W.-H. Shen and D.-Q. Che, *Org. Process Res. Dev.*, 2013, **17**, (2), 307–312

Two processes for the preparation of rivastigmine *via* asymmetric hydrogenation using the chiral spiro catalyst Ir-(*S*)-SpiroPAP-3-Me, **1**, have been developed. The first route was easy to scale up and provided (*S*)-3-(1-dimethylaminoethyl)phenol, which is a suitable intermediate for the manufacture of rivastigmine in API demand. The second route was convenient for operation and purification, giving rivastigmine in four steps in 84% overall yield.

P.-C. Yan *et al.*, *Org. Process Res. Dev.*, 2013, **17**, (2), 307–312

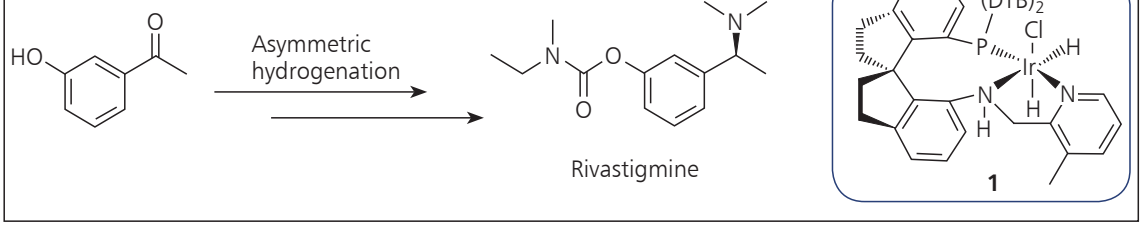

FUEL CELLS

Platinum Monolayer Electrocatalysts: Tunable Activity, Stability, and Self-Healing Properties

R. R. Adzic, *Electrocatalysis*, 2012, **3**, (3–4), 163–169

Pt monolayer nanostructured electrocatalysts were developed for the ORR. These were nm scale core–shell particles with monolayers of Pt supported by metal, metal alloy or nanostructured noble metal/non-noble metal cores. In addition to an ultralow Pt content (one monolayer) and high Pt utilisation (all atoms can participate in the reaction), these catalysts exhibited very high activity and stability induced by the supporting NP cores, by the ability to tune the catalytic activity of the Pt monolayer depending on the properties of the top atomic layer of the cores, and by self-healing. Examples of tunable activity include a Pt monolayer on smooth core surfaces, Pd tetrahedral NPs, Pd nanowire and hollow Pd NP cores.

Electrochemical Properties of Pt/Graphene Intercalated by Carbon Black and Its Application in Polymer Electrolyte Membrane Fuel Cell

S. H. Cho, H. N. Yang, D. C. Lee, S. H. Park and W. J. Kim, *J. Power Sources*, 2013, **225**, 200–206

Graphene single nanosheets (GNSs) were prepared and Pt NPs were shown to be uniformly dispersed on them. The prepared Pt/GNS showed a higher electrochemically active surface area (ECSA) compared to Pt/carbon black and Pt/Vulcan XC-72 CB. Because of significant restacking, different amounts of CB were intercalated between the Pt/GNS as a spacer. The ECSA depended on the content of intercalating compound; Pt/GNS/CB with 30% CB had the highest ECSA of 38.8 $m^2 g^{-1}$ and the best cell performance of 400 mA cm^{-2}.

METALLURGY AND MATERIALS

High-Temperature Mechanical and Shape Memory Properties of TiPt–Zr and TiPt–Ru Alloys

A. Wadood, M. Takahashi, S. Takahashi, H. Hosoda and Y. Yamabe-Mitarai, *Mater. Sci. Eng.: A*, 2013, **564**, 34–41

To try to improve the shape memory properties and strength of Ti-50Pt (in at%) alloys at high temperature, the effects of partial substitution (e.g. 5 at%) of Ti with Zr and of Pt with Ru were investigated. The compressive strength and shape memory properties at high temperature were improved by these partial substitutions, e.g.: 1468 MPa for TiPt–Zr, 712 MPa for TiPt–Ru and 485 MPa for TiPt alloys. Furthermore, Ti-50Pt-5Zr alloy exhibited much higher strength and a better shape memory effect than Ti-45Pt-5Ru alloy.

APPARATUS AND TECHNIQUE

Temperature-Activated Reverse Sensing Behavior of Pd Nanowire Hydrogen Sensors

D. Yang, L. Valentín, J. Carpena, W. Otaño, O. Resto and L. F. Fonseca, *Small*, 2013, **9**, (2), 188–192

H_2 sensors based on individual Pd nanowires (NWs) were fabricated by integrating Pd NWs across microelectromechanical system electrodes, followed by assembling and bonding them to a chip carrier platform. Measurements with these sensors showed reverse sensing behaviours between the temperature zones 370–263 K and 263–120 K.

CHEMISTRY

From Osmium Hydrido Vinylidene to Osmacycles: The Key Role of Osmabutadiene Intermediates

Q. Zhao, X.-Y. Cao, T. B. Wen and H. Xia, *Chem. Asian J.*, 2013, **8**, (1), 269–275

Os hydrido vinylidene, **2**, showed diverse cyclisation reactivity with activated terminal alkynes. Treatment of **2** with HC≡CCOR′ (R′ = OEt and Me) gave osmafurans *via* osmium alkenyl/vinylidenes. Also, **2** reacted with HC≡CCH(OH)C≡CH to yield an osmabenzene, in which the alkynol acted as a C_5 fragment to cyclise with **2**.

Q. Zhao *et al.*, *Chem. Asian J.*, 2013, **8**, (1), 269–275

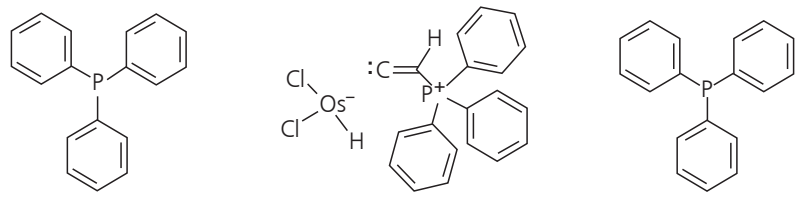

2

Complexation to $[Ru(bpy)_2]^{2+}$: the Trick to Functionalize 3,3′-Disubstituted-2,2′-Bipyridine

P. Guillo, O. Hamelin, J. Pécaut and S. Ménage, *Tetrahedron Lett.*, 2013, **54**, (8), 840–842

The synthesis and chemical transformations of *x*,*x*′-disubstituted-2,2′-bipyridine with x = 4, 5 or 6 are often reported. This is not the case when x = 3. Several [(2,2′-bipyridine)$_2$Ru(3,3′-dialkylated-2,2′-bipyridine)]$^{2+}$ complexes were prepared highlighting surprising chemical behaviour by the 3,3′-disubstituted-2,2′-bipyridine ligand.

ELECTRICAL AND ELECTRONICS

Spin Wave-Assisted Reduction in Switching Field of Highly Coercive Iron-Platinum Magnets

T. Seki, K. Utsumiya, Y. Nozaki, H. Imamura and K. Takanashi, *Nature Commun.*, 2013, **4**, (4), 1726

Extremely low-field magnetisation switching was experimentally demonstrated in highly coercive FePt by using a spin wave excited in a soft magnetic permalloy ($Ni_{81}Fe_{19}$), where the permalloy was exchange-coupled to FePt through the interface. The switching field could be tuned by varying the magnitude and frequency of the radio frequency magnetic field, and a decrease in switching field by one order of magnitude was achieved under optimum conditions. Spin wave-assisted magnetisation switching is therefore promising as an ultralow-energy magnetisation manipulation technique.

PHOTOCONVERSION

A Deep-Blue Emitting Charged Bis-cyclometallated Iridium(III) Complex for Light-Emitting Electrochemical Cells

S. B. Meier, W. Sarfert, J. M. Junquera-Hernández, M. Delgado, D. Tordera, E. Ortí, H. J. Bolink, F. Kessler, R. Scopelliti, M. Grätzel, M. K. Nazeeruddin and E. Baranoff , *J. Mater. Chem. C*, 2013, **1**, (1), 58–68

A cationic Ir(III) complex showed deep-blue emission in a concentrated film and could be used in light-emitting electrochemical cells (LECs). The complex was based on the 2′,6′-difluoro-2,3′-bipyridine skeleton as the cyclometallating ligand and a bis-imidazolium carbene-type ancillary ligand; bulky *tert*-butyl substituents were used to limit the intermolecular interactions. LECs were driven both at constant voltage (6 V) and constant current (2.5 mA cm^{-2}). The performances were significantly improved with the latter method.

Ruthenium Complex Dye with Designed Ligand Capable of Chelating Triiodide Anion for Dye-Sensitized Solar Cells

J.-S. Ni, K.-C. Ho and K.-F. Lin, *J. Mater. Chem. A*, 2013, **1**, (10), 3463–3470

Ru(4,4′-dicarboxyl-2,2′-bipyridine)[4,4′-bis(styrylaminocarbonyl)-2,2′-bipyridine](NCS)$_2$ was synthesised. Its ability to chelate triiodide anions with the 4,4′-bis(styrylaminocarbonyl)-2,2′-bipyridine ligand reduced charge recombination for DSSCs by keeping the triiodide ions away from the mesoporous TiO_2 layer. The open-circuit photovoltage of the DSSC barely changed with the triiodide concentration in the electrolyte. The electron-withdrawing ability of the amide groups in the ligand increased the molar extinction coefficient of the dye, leading to an increase of photocurrent for the DSSCs.

Wideband Dye-Sensitized Solar Cells Employing a Phosphine-Coordinated Ruthenium Sensitizer

T. Kinoshita, J. T. Dy, S. Uchida, T. Kubo and H. Segawa, *Nature Photon.*, 2013, doi:10.1038/nphoton.2013.136

Efficient DSSCs that exploit near-IR spin-forbidden singlet-to-triplet direct transitions in a phosphine-coordinated Ru(II) sensitiser, DX1, were fabricated. A DSSC using DX1

generated a photocurrent density of 26.8 mA cm^{-2}. A tandem-type DSSC employing both DX1 and the sensitiser N719 was shown to have a power conversion efficiency of >12% under 35.5 mW cm^{-2} simulated sunlight.

REFINING AND RECOVERY

Recovering Palladium from Its Surplus Complexes in Research Laboratories by Solid State Thermal Treatment

J. Pérez, J. L. Serrano, J. E. Granados and L. A. Alcolea, *RSC Adv.*, 2013, **3**, (14), 4558–4567

A method for the recovery of Pd from research laboratory wastes is based on heating Pd complexes to 900ºC in a dynamic air atmosphere to get a Pd residue of purity ~95%. The purity of the metal in the final residue depended on the nature of the Pd complexes; when the sample did not contain P ligands the recovery of Pd was stoichiometric. This was thought to be related to the remarkable inhibition of PdO formation exerted under these conditions by P ligands, free or coordinated to Pd, that was observed in this study.

